2017 IEEE Intelligent Vehicles Symposium (IV)
June 11-14, 2017, Redondo Beach, CA, USA

Path Following Control for Autonomous Formula Racecar: Autonomous Formula Student Competition

Jun NI, *Member, IEEE*, Jibin HU

***Abstract*—This paper summarizes our work of an envelope path following controller for a four-wheel independently actuated (FWIA) autonomous racecar. The controller consists of three modules through the integrated control of active front-wheel steer (AFS) and direct yaw-moment control (DYC). An electric autonomous Formula Student racecar is used as testbed to test the controller Moreover, the Formula Student competition is introduced. With the cooperation with SAE China, the authors are trying to establish the autonomous Formula Student racecar competition in China. In this paper, the basic concept and rules of autonomous Formula Student racecar competition is described.**

***Index Terms*—Autonomous Vehicle; Electric Vehicle; Path Following; Formula Student; Autonomous Racecar.**

I. Introduction

Formula Student racecar competition is a popular competition between worldwide universities, which is organized by Society of Automotive Engineering (SAE) and Institution of Mechanical Engineers (IMechE). This competition is very popular in U.S.A, Europe and China, which encourages students to design, build and compete with a Formula-style racecar. The competition is split into static and dynamic events. Static events include business presentation, cost report and design report. Dynamic events include acceleration, skid pad, autocross, endurance and fuel economy [1]. Currently, Formula Student competition consists of 'Combustion' and 'Electric' competitions. The author of this paper used to sever as the team captain of the Beijing Institute of Technology Formula Student racecar team.

Recently, autonomous driving technology has attracted increasing focus in both academic and industry field [2,3]. As a famous competition for education purpose, it's necessary for Formula Student competition to involve autonomous driving competition. Therefore, the authors are helping SAE China to establish the autonomous Formula Student competition. This paper reported our recent work on a Formula Student racecar, which mainly deals with the path following and dynamics control topic. There have been many path following controllers proposed for AGV in literatures [4-10]. Recently, the emergence of FWIA drive technique provides potentials to significantly improve the path following performance for AGV. C. Hu combined Active Front Steer (AFS) and Direct Yaw Control (DYC) to design a controller based on back step -ping method, which aims to both stabilizing the path error and considering the lateral offset constraint [11]. R. Wang proposed a composite nonlinear controller for FWIA AGV to improve the transient performance considering tire saturations, in presence of time-varying road curvature [12].

Moreover, in academic point of view, there are still insufficiencies need to be addressed: 1) The integrated control of AFS and DYC provides great potentials to follow the desired path and simultaneously travel at its driving limits to minimize the maneuver time. Little research has focused on it. 2) The experimental validation based on a real AGV, which adopts AFS and DYC integrated control, has been seldom reported. To this end, this paper describes the basic concept and rules of autonomous Formula Student racecar competition. Based on it, a path following controller to regulate it on desired path and control it to the driving limits simultaneously is proposed and validated by the experiments.

II. Concept of Autonomous Formula Student Competition

Formula Student competition is very popular in U.S.A, Europe and China, which is a famous education event to encourage the students to design, build and compete with a Formula-style racecar. Figure 1 shows the pictures of all teams in 2015 Formula Student Germany and 2016 Formula Student China. Take them as examples, there are over 120 teams from the universities around the world participate in Formula Student Germany every year. Currently, the Formula Student includes the competitions for combustion and electric racecars. Figure 2 shows a combustion and an electric racecars developed by BIT team in 2013 and 2015 respectively.

(a) Formula Student in Germany

(b) Formula Student in China

Fig.1 Pictures of All Teams in Formula Student Competition

(a) Combustion Racecar

(b) Electric Racecar

Fig.2 Formula Student Racecars Developed by BIT Team in 2013 and 2015

It is supported by the National Natural Science Foundation of China under Grant U1564210.

Jun NI is visiting scholar with Mechanical Engineering Department, University of California, Berkeley. (nijun_bit@163.com).

Jibin HU is with School of Mechanical Engineering, Beijing Institute of Technology, China.

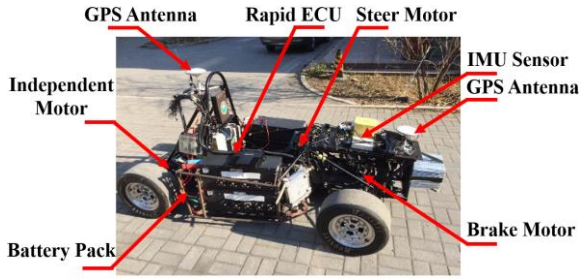

Fig.3 The Autonomous Formula Student Racecar Developed by the Authors

The combustion racecar is driven by engine, and the electric racecar is driven by electric motors. As above mentioned, the autonomous driving technology has attracted increasing focus in both academic and industry fields. Based on the experience in Formula Student racecar design, the authors developed the first autonomous Formula Student racecar in the world as Figure 3 shown. It is modified based on a former electric racecar. Its total mass is 400kg with maximum speed as 110km/h. Figure 3 shows its hardware configuration. Each rear wheel is independently driven by a motor, which is mounting in the vehicle body. The maximum power of each independent motor is 60kW. The vehicle is powered by LiFePo4 battery pack, and the battery voltage is 400V with 8kWh capacity. The steering and braking system is controlled by servomotors. A Differential GPS/INS system and two antennas are equipped. Actually, there have been several successful autonomous prototype vehicles developed in the world, especially the P1, X1 and Shelley in Stanford University [9,10].

Recently, the authors are helping SAE China to establish the autonomous Formula Student competition in China. The basic events include remote control event, path following event with a given path and autonomous event. These three level events are step-by-step. The remote control event is the lowest level, which is easy to be achieved for all the teams. The remote control event is to compete with the human operator in loop with remote control technique. The path following event means the path will be given by the committee through GPS data, and the racecars are supposed to finish the given path to see who is the fastest. Its purpose is to test the dynamics control technique of the autonomous racecar. The autonomous event is the highest level. Apparently, it means all the racecars should detect the environments and finish the racetrack by themselves. The detail of the competition will be presented in the conference.

III. G-G Diagram

This paper focuses on the path following to control the vehicle to follow the desired path and simultaneously travel at its driving limits, which is a key technique of autonomous racecar. At first, the G-G diagram to should be introduced to represent the driving limits of the vehicle.

Figure 4 shows the calculated G-G diagram of the autonomous Formula Student racecar shown in Figure 3. The detail of the calculation process can be seen in our previous work [13]. G-G diagram is often used to obtain accurate observation of vehicle limits. It plots longitudinal acceleration (vertical axis) against lateral acceleration (horizontal axis) with origin point locating on the middle of the diagram. The boundary of the G-G diagram represents the maximum acceleration capability of the vehicle.

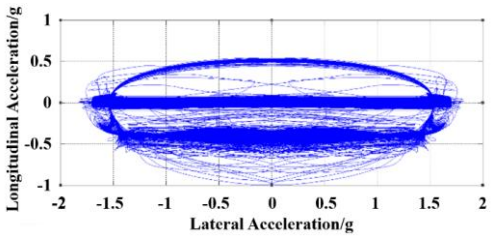

Fig 4. Calculated G-G Diagram of the Autonomous Racecar Testbed

According to Fig. 4, it can be observed that the maximum positive and negative acceleration of the race car is 0.5 and 1g, and the maximum lateral acceleration is 1.8g. The boundary lines in 1st and 2nd quadrants show the acceleration capability when the race car is accelerating out of the corner, and the boundary lines in 3rd and 4th quadrants show when it's braking into the corner.

IV. Envelope Path Following Controller

Envelope control technique has been implemented successfully in aircraft for last decades to keep the aircraft within a safe region [14]. In our work, the envelope control concept is applied to path following control.

A. Overall Controller Architecture

Fig. 5 shows the overall architecture of envelope controller, which consists of longitudinal, lateral and yaw controllers. The speed controller aims at calculating the desired total traction or braking force according to the driving speed limit calculated by pre-defined G-G diagram boundary and desired path. The path following controller aims at minimizing the error between actual and desired path. To assure the handling stability during the maneuver under limit condition, a yaw moment controller is designed through sliding mode control technique according to pre-defined safe β-r phase portraits. In this paper, the envelopes used in the proposed controller include G-G diagram and β-r phase portraits.

B. Path Description

This paper focuses on the path following control. Therefore, the desired path will be directly given. Clothoid path description method is applied in this paper which is widely used in highway road design [15]. The curvature along the path can be described:

$$k(s) = 2c^2 s_i \tag{1}$$

According to (1), the desired path can be given as Figure 6 shows. To achieve driving limits, the path example is given according to racecar driver's driving technology, which sepa

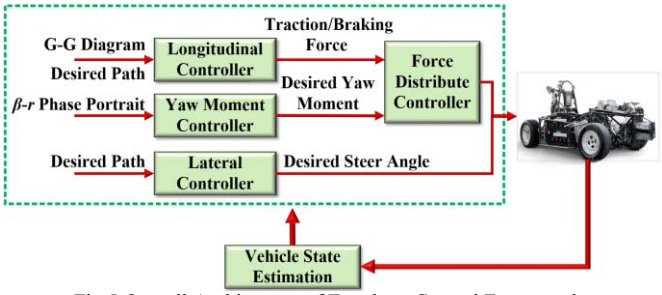

Fig.5 Overall Architecture of Envelope Control Framework

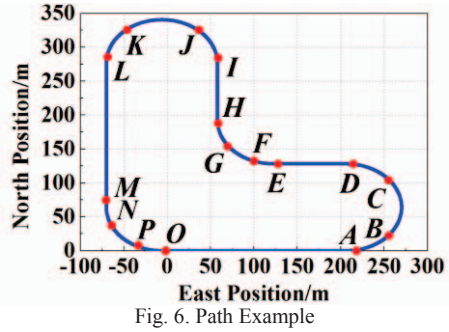

Fig. 6. Path Example

-rates each corner sequence into a corner entry, an apex (constant radius) and a corner exit. According to Figure 6, assume the racecar starts at point O. During straightline OA, the vehicle accelerates at the highest longitudinal acceleration and then brakes at the highest negative acceleration to go into the corner. AB indicates the corner entry and the vehicle is supposed to brake into the corner and operate through the boundary line on 3rd or 4th quadrants in G-G diagram. BC indicates the constant radius corner apex when the vehicle needs to operate at the highest lateral acceleration. CD indicates the corner exit when the vehicle is supposed to accelerate out of the corner and operate through the boundary line on 1st or 2nd quadrants in G-G diagram. The other three corners EFGH, IJKL and MNPO is the same.

C. Longitudinal Controller

The speed profile is obtained according to the G-G diagram boundary and desired path curvature information along the path segment. A feedforward controller is designed based on the speed profile, and a feedback controller is designed according to the error between speed profile and actual speed feedback.

Assume the G-G diagram boundary shown in Fig. 4 could be expressed by two half oval assumption:

$$\begin{cases} \frac{1}{\lambda^2}\left(\frac{a_x^2}{a_{y\max}^2}+\frac{a_y^2}{a_{x\max T}^2}\right)=1\ ,\ a_x>0 \\ \frac{1}{\lambda^2}\left(\frac{a_x^2}{a_{y\max}^2}+\frac{a_y^2}{a_{x\max B}^2}\right)=1\ ,\ a_x<0 \end{cases} \tag{2}$$

Where a_{ymax} is the maximum ideal lateral acceleration of simulated G-G diagram. a_{xmaxT} is the maximum ideal positive longitudinal acceleration. a_{xmaxB} is the maximum ideal negative longitudinal acceleration. λ is the adjust parameter according to the change of the tyre-road friction coefficient.

According to the G-G diagram boundary shown in (2) and the desired path, the speed profile could be determined. The main procedure is shown here. Assume the vehicle starts at point O and moves anticlockwise. The desired speed at corner apex BC should be calculated firstly. At corner apex BC, the vehicle is supposed to operate at maximum lateral acceleration where a_x=0 and a_y=λa_{ymax}. The desired speed at corner apex BC could be calculated as:

$$U_x(s)=\sqrt{\lambda a_{y\max}R} \tag{3}$$

After the speed profile along corner apex BC is determined, the speed profile along corner entry AB could be calculated. In corner entry AB, the vehicle is supposed to trace the boundary of 3rd or 4th quadrant of the G-G diagram with both negative longitudinal and lateral acceleration acting. When the vehicle is in AB, the lateral acceleration can be calculated:

$$a_y=2c^2sU_x^2(s) \tag{4}$$

The desired negative acceleration can be calculated as:

$$a_x(s)=\sqrt{\frac{a_{x\max B}^2a_{y\max}^2\lambda^2-a_{y\max}^2[U_x(s)^2 2c^2s]^2}{a_{x\max B}^2}} \tag{5}$$

Equation (5) cannot be solved because U_x(s) is unknown. Consider following equation:

$$a_x(s)=\frac{dU_x(s)}{dt}=\frac{dU_x(s)}{ds}\frac{ds}{dt}=\frac{dU_x(s)}{ds}U_x(s) \tag{6}$$

Substitute (6) into (5) yields:

$$\frac{dU_x(s)}{ds}=\frac{1}{U_x(s)}\sqrt{\frac{a_{x\max B}^2a_{y\max}^2\lambda^2-a_{y\max}^2(U_x(s)^2 2c^2s)^2}{a_{x\max B}^2}} \tag{7}$$

Equation (7) can be solved based on backward integration. After the desired speed along AB segment is obtained, the desired speed at point A can be obtained as U_A. In straightline OA, the vehicle is supposed to firstly accelerate with the maximum positive longitudinal acceleration and then brake with the maximum negative longitudinal acceleration at an appropriate point to achieve U_A at point A. After the desired speed along the straightline OA is determined. The desired speed profile along OC has been obtained. The desired speed in the corner exit CD can be calculated like the corner entry AB case. The calculation procedures of left path segments are the same as above. Once the desired speed and desired longitudinal acceleration along all the path segments is known, the feedforward longitudinal force could be obtained. A feedback controller is added according to the error between desired and actual speed.

$$F_{xd}=ma_x(s)+K_1[U_{xa}(s)-U_{xd}(s)] \tag{8}$$

Where U_{xa}(s) is the actual vehicle speed, U_{xd}(s) is the desired vehicle speed. K_1 is the feedback gain. The total longitudinal force is equally distributed to the independent motors' torque.

D. Lateral Controller

The error dynamics is shown in Fig. 7. The projected error e_p is used to combine lateral error e and heading error $\Delta\Phi$. The relationship of the kinematics parameters is shown:

$$\begin{cases} \dot{e}=U_y\cos\Delta\phi+U_x\sin\Delta\phi \\ e_p=e+x_p\sin\Delta\phi \\ \Delta\phi=\phi-\phi_p \\ \Delta\dot{\phi}=\dot{\phi}-\dot{\phi}_p=r-\kappa\dot{s} \end{cases} \tag{9}$$

The 2DOFs vehicle dynamics model will be used to design the lateral controller, which is expressed as following:

$$\begin{cases} \dot{\beta}=a_{11}\beta+a_{12}r+b_{11}\delta \\ \dot{r}=a_{21}\beta+a_{22}r+b_{21}\delta \end{cases} \tag{10}$$

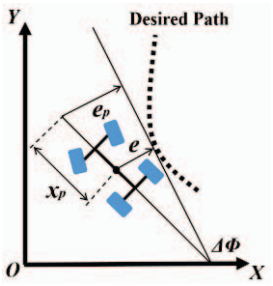

Fig. 7. Path Following Model

Where r is the yaw velocity. β is the side slip angle. δ is the steer angle. According to small angle approximation, it could be assumed that $\Delta\Phi = \sin\Delta\Phi = \cos\Delta\Phi$. Assume $U_y\cos\Delta\Phi$ is small enough to be neglected. The error dynamics model could be written according to (9) and (10):

$$\dot{X} = AX + B\delta + \tilde{P} \tag{11}$$

Where:

$$X = \begin{bmatrix} e \\ \Delta\phi \\ \beta \\ r \end{bmatrix}, A = \begin{bmatrix} 0 & U_x & 0 & 0 \\ 0 & 0 & 0 & 1 \\ 0 & 0 & a_{11} & a_{12} \\ 0 & 0 & a_{21} & a_{22} \end{bmatrix}, B = \begin{bmatrix} 0 \\ 0 \\ b_{11} \\ b_{21} \end{bmatrix}, \tilde{P} = \begin{bmatrix} 0 \\ -\kappa\dot{s} \\ 0 \\ 0 \end{bmatrix} \tag{12}$$

The matrix elements are defined as:

$$\begin{cases} a_{11} = \dfrac{c_f + c_r}{mU_x}, a_{12} = -1 + \dfrac{l_f c_f - l_r c_r}{mU_x^2} \\ a_{21} = \dfrac{l_f c_f - l_r c_r}{I_z}, a_{22} = \dfrac{l_f^2 c_f + l_r^2 c_r}{I_z U_x} \\ b_{11} = \dfrac{-c_f}{mU_x}, b_{21} = \dfrac{-l_f c_f}{I_z} \end{cases} \tag{13}$$

Where $\tilde{P}$ can be considered as the disturbance from the curvature. The feedforward controller aims at eliminating $\ddot{e}_p$. Adopt same assumptions before (11), it could be obtained:

$$\dot{e}_p = \dot{e} + x_p\Delta\dot{\phi} = U_x\Delta\phi + x_p(r - \kappa\dot{s}) \tag{14}$$

Assume $U_x\dot{\Delta\Phi}=0$, then it could be obtained:

$$\ddot{e}_p = U_x\Delta\dot{\phi} + x_p(\dot{r} - \dot{\kappa}\dot{s} - \kappa\ddot{s}) = U_x r - U_x\kappa\dot{s} + x_p\dot{r} - x_p(\kappa\ddot{s} + \dot{\kappa}\dot{s}) \tag{15}$$

The goal of feedforward lateral controller is:

$$\lim_{t\to\infty}\ddot{e}_p = 0 \tag{16}$$

By equating (15) to zero, it could be obtained:

$$U_x r - U_x\kappa\dot{s} + x_p(a_{21}\beta + a_{22}r + b_{21}\delta) - x_p(\kappa\ddot{s} + \dot{\kappa}\dot{s}) = 0 \tag{17}$$

The feedforward δ could be solved:

$$\delta_{FFW} = \frac{-U_x r - x_p a_{21}\beta - x_p a_{22} r + U_x\kappa\dot{s} + x_p(\kappa\ddot{s} + \dot{\kappa}\dot{s})}{x_p b_{21}} \tag{18}$$

The feedback lateral controller is obtained according to projected error e_p. The yaw dynamics becomes more oscillatory since the damping ratio decreases because the tyre adhesion capability decreases in limit condition. A small amount of yaw damping is adding to the controller.

$$\delta_{FB} = -K_2 e_p - K_3\dot{\Delta\phi} \tag{19}$$

The total steering angle is $\delta_{FFW}+\delta_{FB}$. Substitute it into (19), and final closed-looped model could be obtained:

$$\dot{X} = \hat{A}X + \hat{P} \tag{20}$$

Where:

$$\hat{A} = \begin{bmatrix} 0 & u & 0 & 0 \\ 0 & 0 & 0 & 1 \\ -b_{11}K_2 & -b_{11}K_2 x_p & a_{11} - \dfrac{b_{11}a_{21}}{b_{21}} & a_{12} - \dfrac{b_{11}U_x}{x_p b_{21}} - \dfrac{b_{11}a_{22}}{b_{21}} - b_{11}K_3 \\ -b_{21}K_2 & -b_{21}K_2 x_p & 0 & -\dfrac{U_x}{x_p} - b_{12}K_3 \end{bmatrix} \tag{21}$$

Define a Lyapunov function for the system in (25):

$$V = X^T Q X \tag{22}$$

If a matrix Q exists such that V is positive and $\dot{V}=X^T(\hat{A}^T Q+Q\hat{A})X$ is negative for all non-zero X, then the system is stable. The requirements for the system stability can be written as $Q>0$ and $\hat{A}^T Q+Q\hat{A}<0$. The disturbance $\hat{P}$ is caused by the curvature and it is bounded. $\dot{s}$ and $\ddot{s}$ is bounded by the U_x and a_x. Define parameter η_f and η_r to represent the change of front and rear tyre cornering stiffness, the actual tyre cornering stiffness could be expressed by $\eta_f c_f$ or $\eta_r c_r$. The value of η_f and η_r varies from zero to one. To discuss the stability when η_f changes, $\hat{A}$ could be written as a convex combination of $\hat{A}_{0f}$ and $\hat{A}_{1f}$.

$$\hat{A} = \hat{A}_{0f} + \eta_f\hat{A}_{1f} \tag{23}$$

Where:

$$A_{0f} = \begin{bmatrix} 0 & u & 0 & 0 \\ 0 & 0 & 0 & 1 \\ 0 & 0 & 0 & \dfrac{-l_r c_r - mU_x^2}{mU_x^2} - \dfrac{I_z}{mx_p l_f} - \dfrac{l_r^2 c_r}{mU_x^2 l_f} \\ 0 & 0 & 0 & -\dfrac{U_x}{x_p} \end{bmatrix} \tag{24}$$

$$A_{1f} = \begin{bmatrix} 0 & 0 & 0 & 0 \\ 0 & 0 & 0 & 0 \\ \dfrac{c_f K_2}{mU_x} & \dfrac{c_f K_2 x_p}{mU_x} & \dfrac{c_f L}{mU_x l_f} & \dfrac{l_f c_f}{mU_x^2} - \dfrac{l_f^2 c_f}{mU_x^2 l_f} + \dfrac{c_f K_3}{mU_x} \\ \dfrac{l_f c_f K_2}{I_z} & \dfrac{l_f c_f K_2 x_p}{I_z} & 0 & \dfrac{l_f c_f K_3}{I_z} \end{bmatrix} \tag{25}$$

Consequently, $\hat{A}^T Q+Q\hat{A}<0$ can be written as:

$$\hat{A}^T Q + Q\hat{A} = \hat{A}_{0f}^T Q + QA_{0f} + \eta_f(\hat{A}_{1f}^T Q + QA_{1f}) \tag{26}$$

If a positive Q is found such that (26) is satisfied, then the system during the range of $\eta_f(0\le\eta_f\le1)$ is stable:

$$\begin{cases} \hat{A}_{0f}^T Q + Q A_{0f} + \eta_{f\min}(\hat{A}_{1f}^T Q + Q A_{1f}) < 0 \\ \hat{A}_{0f}^T Q + Q A_{0f} + \eta_{f\max}(\hat{A}_{1f}^T Q + Q A_{1f}) < 0 \end{cases} \quad (27)$$

Similarly, to discuss the stability when η_r changes, the same procedure can be made. The positive matrix Q that satisfies (27) can be found by Matlab's Linear Matrix Inequality (LMI) solver. The results show that, in each speed case, a positive matrix Q can always be found. To improve the robustness, the tyre cornering stiffness will be estimated with the convenience of FWIA EV. The tyres of the autonomous race car testbed have been tested by test-rig and the Magic Formula model has been obtained. Based on the predefined Magic Formula model, the tyre cornering stiffness can be estimated online, and the details can be seen in [16].

E. Yaw Moment Controller

The yaw moment controller aims at assuring the handling stability during the limit maneuver. As part of envelope control concept, the safe β-r phase portrait envelopes are utilized. In our work, the β-r phase portraits are calculated by Magic Formula model and 2DOFs dynamic model. The detail of the safe boundary will be omitted due to the space limitation. In each condition, the safe boundary of phase portraits can be defined by a parallelogram as Fig. 8 [17].

Fig. 8 shows the parallelogram boundary in example condition when vehicle speed is 15m/s and steering angle is zero. In other conditions, the safe boundary can be expressed with similar parallelograms and expressions of each lines are:

$$\begin{cases} QT: \beta = b_0 r + b_1, RS: \beta = b_0 r - b_1 \\ RQ: r = b_2 \beta + b_3, ST: r = b_2 \beta - b_3 \end{cases} \quad (28)$$

The details of the parameters b_0, b_1, b_2, b_3 can be seen in literature [17]. They are functions of vehicle configuration pa rameters, vehicle speed U_x and steer angle δ. The influence of U_x and δ on the boundary shape is reflected by these parameters. After the safe envelopes are determined, a sliding mode controller can be applied to generate active yaw moment. The sliding surface is defined as:

$$S = (r - r_{safe}) - q(\beta - \beta_{safe}) \quad (29)$$

The design process of the sliding surface controller is quite common, which will be omitted in this paper. Some details can be seen in [17].

V. Experiment Results

The autonomous electric Formula Student racecar shown in Figure 3 is used to test the proposed controller. The path shown in Figure 6 is used as desired path, which is written into the ECU controller through GPS/INS system. The tyre-warm laps are conducted to warm the tyres up before the autonomous experiments. It is necessary to make the tyres operate in the best temperature to provide the possibility for the racecar to fully operate on the boundary of G-G diagram. The experiment results are shown following.

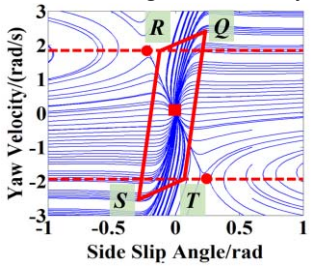

Figure 8. Example of Safe Boundary

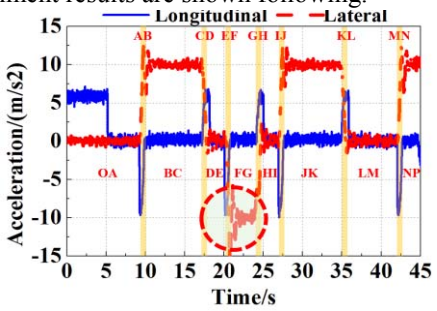

Fig.9. Longitudinal and Lateral Acceleration

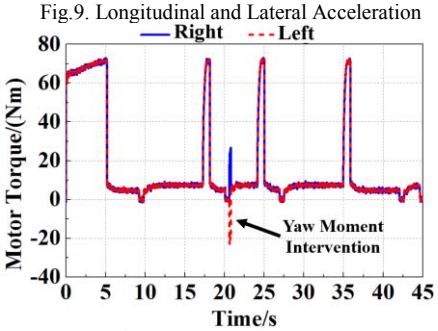

Fig.10. Torque of Each Motor

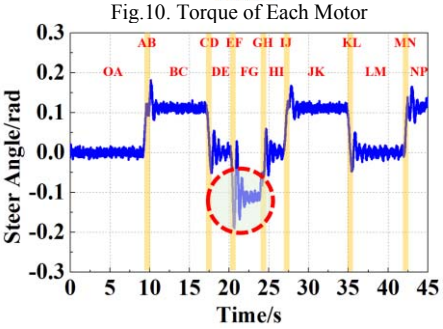

Fig.11. Steer Angle

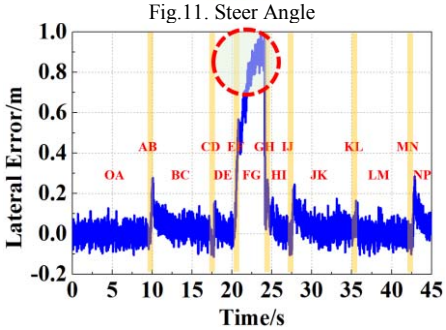

Fig.12. Lateral Error

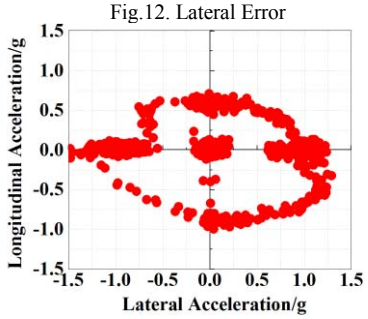

Fig.13. G-G Diagram

In straightline OA, the independent motors provide maximum torque as about 70Nm to achieve the maximum acceleration, and the vehicle achieves maximum speed at 5s. At 9s, the vehicle brakes at the maximum negative acceleration to go into the corner entry AB. The maximum positive and negative longitudinal acceleration achieves about 0.7g and -1.0g. The lateral error increases during corner entry AB, which peaks about 0.3m. It can be seen in Fig. 13, the points in 4th quadrant basically match the boundary of the 4th quadrant of the target G-G diagram. In corner apex BC, the vehicle is operating at the maximum lateral acceleration as about 1.1-1.3g. The steer angle is about 0.1rad. The lateral error decreases to almost zero after the transition during AB. In corner exit CD, the vehicle is controlled to operate at the boundary of the 2nd quadrant of the target G-G diagram. The longitudinal acceleration gradually increases and the lateral acceleration gradually decreases. In straightline DE, the vehicle is operating at highest speed.

Then the vehicle brakes into corner entry EF. But the vehicle loses stability during this transition maneuver. At about 20.4s, the vehicle begins to spin. It can be seen that the vehicle motion variables fluctuate a lot after the spin occurs and these phenomenon are marked by red circles in the figures. The yaw moment controller is triggered to keep the stability. It can be seen that the peak torque value of left motor is about 28Nm and the peak torque value of right motor is about -22Nm. After the sudden yaw moment is input, the vehicle becomes stable again. It can be concluded that the yaw moment controller successfully prevents the vehicle from completely losing the stability. Actually, the radius of the corner entry EF and corner apex FG is same as other corner entries and corner apexes. The only difference is that the corner EFGH is a right hand turn. The reason of the vehicle to lose stability in this corner may be because of the asymmetry of the vehicle configuration or mass distribution between half and right parts, or the adjustment difference of tyre camber between half and right suspensions.

VI. CONCLUSION

This paper reported the work about establishing the autonomous Formula Student competition. Besides combustion and electric competitions, the autonomous racecar competition will be a great new event in Formula Student family. The autonomous Formula Student racecar developed by the authors is introduced. Moreover, to deal with the path following topic of the autonomous racecar, this paper summarizes our work about the envelop path following controller design, which provides the possibility for the autonomous racecar to follow the desired path and simultaneously travel at its limits. The experiment results on a given path is shown to validate the controller.

REFERENCES

[1] Formula SAE rules, SAE International, Warrendale, Pennsylvania, USA, 2007, available from http://www.sae.org.

[2] P. Kachroo, S. Sastry. "Travel Time Dynamics for Intelligent Transportation Systems: Theory and Applications," *IEEE Trans. Intell. Transp. Syst.*, vol. 17, no. 2, pp. 385-394, 2016.

[3] K. C. Dey, L. Yan, X. Wang, et al. "A Review of Communication, Driver Characteristics and Controls Aspects of Cooperative Adaptive Cruise Control," *IEEE Trans. Intell. Transp. Syst.*, vol. 17, no. 2, pp. 491-509, 2016.

[4]J. Yang, E. Hou, M. Chu. "Front Sensor and GPS-based Lateral Control of Automated Vehicles," *IEEE Trans. Veh. Technol.*, vol. 14, no. 1, pp. 146–154, 2013.

[5]P. Falcone, F. Borrelli, J. Asgari. "Predictive Active Steering Control for Autonomous Vehicle Systems," *IEEE Trans. Control syst.*, vol. 15, no. 3, pp. 566–580, 2007.

[6]Y. S. Son, W. Kim and S. Lee. "Robust Multirate Control Scheme with Predictive Virtual Lanes for Lane Keeping System of Autonomous Highway Driving," *IEEE Trans. Veh. Technol.*, vol. 64, no. 8, pp. 3378–3391, 2015.

[7]H. Yang, V. Cocquempot, B. Jiang. "Optimal Fault Tolerant Path Tracking Control for 4WS4WD Electric Vehicles," *IEEE Trans. Intell. Transp. Syst.*, vol. 11, no. 1, pp. 1643-1656, 2010.

[8]A. Gray, M. Ali, Y. Gao., et al. "A Unified Approach to Threat Assessment and Control for Automotive Active Safety," *IEEE Trans. Intell. Transp. Syst.*, vol. 14, no. 3, pp. 1490-1499, 2013.

[9]K. Talvala, K. Kritayakirana, J. C. Gerdes. "Pushing the Limits: From Lankeeping to Autonomous Racing," *Annual Reviews in Control*, vol. 35, pp. 137-148, 2011.

[10]K. Kritayakirana, J. C. Gerdes. "Using the Centre of Percussion to Design a Steering Controller for an Autonomous Race Car," *Vehicle System Dynamics*, vol. 50, pp.33-51, 2012.

[11]C. Hu, R. Wang, F. Yan., et al. "Output Constraint Control on Path Following of Four-wheel Independently Actuated Autonomous Ground Vehicles," *IEEE Trans. Veh. Technol.*, DOI 10.1109/TVT.2015. 24729 75.

[12]R. Wang, C. Hu, F. Yan, et al. "Composite Nonlinear Feedback Control for Path Following of Four-wheel Independently Actuated Autonomous Ground Vehicle," *IEEE Trans. Intell. Transp. Syst.*, vol. 17, no. 7, pp. 2063-2074, 2016.

[13]J. Ni, et al. "GG Diagram Generation based on Phase Plane Method and Experimental Validation for FSAE Race Car," *SAE 2016 World Congress and Exhibition*, 2016.

[14]M. R. Anderson, W. H. Mason. "An MDO Approach to Control Configured Vehicle Design," *American Institute of Aeronautics and Astronautics*. Paper No. 96-4058.

[15]Aashto. "Green Book: A Policy on Geometric Design of Highways and Streets," American Association of State Highway and Transportation Officials, Washington D.C., USA.

[16]J. Ni, Jibin Hu. "Dynamics control of autonomous vehicle at driving limits and experiment on an autonomous Formula racing car," *Mech. Syst. Signal Process.*, vol. 90, pp. 154–174, 2017.

[17]C. G. Bobier and J. C. Gerdes. "Staying within the Nullcline Boundary for the Vehicle Envelope Control Using a Sliding Surface," *Vehicle System Dynamics*, vol. 48, no.2, pp.199-217, 2013.

[18]J.-J. E. Slotine and W. Li. "Applied Nonlinear Control," New Jersey 07632: Prentice Hall, 1991.